

# Strong electron-phonon coupling, electron-hole asymmetry, and nonadiabaticity in magic-angle twisted bilayer graphene

Young Woo Choi and Hyoung Joon Choi\*

*Department of Physics, Yonsei University, Seoul 03722, Republic of Korea*

(Dated: December 16, 2019)

We report strong electron-phonon coupling in magic-angle twisted bilayer graphene (MA-TBG) obtained from atomistic description of the system including more than 10,000 atoms in the moiré supercell. Electronic structure, phonon spectrum, and electron-phonon coupling strength  $\lambda$  are obtained before and after atomic-position relaxation both in- and out-of-plane. Obtained  $\lambda$  is very large for MA-TBG, with  $\lambda > 1$  near the half-filling energies of the flat bands, while it is small ( $\lambda \sim 0.1$ ) for monolayer and unrotated bilayer graphene. Significant electron-hole asymmetry occurs in the electronic structure after atomic-structure relaxation, so  $\lambda$  is much stronger with hole doping than electron doping. Electron-phonon coupling is nearly isotropic and very weakly dependent on electron momentum, suggesting single-gap *s*-wave superconductivity. Relevant phonon energies are much larger than electron energy scale, going far beyond adiabatic limit. Our results provide fundamental understanding of electron-phonon interaction in MA-TBG, highlighting that it can contribute to rich physics of the system.

Interplay between the interlayer coupling and the rotational mismatch between two graphene layers in bilayer graphene results in flattening of Dirac cones at certain special twist angles  $\theta_M$ , called magic angles [1–3]. Recently, correlated insulator behavior and superconductivity are experimentally observed near the first magic angle  $\theta_M = 1.08^\circ$ , demonstrating rich physics induced by the presence of the flat bands [4, 5]. In this regard, more detailed characterizations for the magic-angle twisted bilayer graphene (MA-TBG) are attracting large interest [6–52].

In addition to the exotic electronic properties, it has been observed that low-angle bilayer graphene exhibits atomic-scale reconstruction [53]. Essential effect of the lattice relaxation is such that the area of AA stacking region becomes smaller, while AB stacking region larger, and this effect becomes more important as the twist angle gets smaller. Also, it is suggested that the lattice relaxation can affect the electronic structure, opening superlattice-induced energy gaps at the band edges on both electron and hole side [54]. Since these gaps are clearly observed in the experiments [4, 55], it is necessary to consider the lattice relaxation when studying TBG in low-angle regime.

As the electron-phonon coupling strength  $\lambda$  in simple monolayer and unrotated bilayer graphene is too weak, superconductivity in MA-TBG is suspected to be originated from the electron correlation. *Ab initio* calculations found that  $\lambda$  of monolayer and unrotated bilayer graphene is less than 0.1 near the charge-neutral Fermi level [56]. If  $\lambda$  has a similar value in MA-TBG, it cannot account for the observed superconducting transition temperature  $T_c \sim 1$  K.

However, since  $\lambda$  is proportional to the electron density of states,  $\lambda$  of AB-stacked bilayer graphene (AB-BLG), for example, can be as large as 0.28 when the Fermi level is tuned to near the van Hove singularity points. This

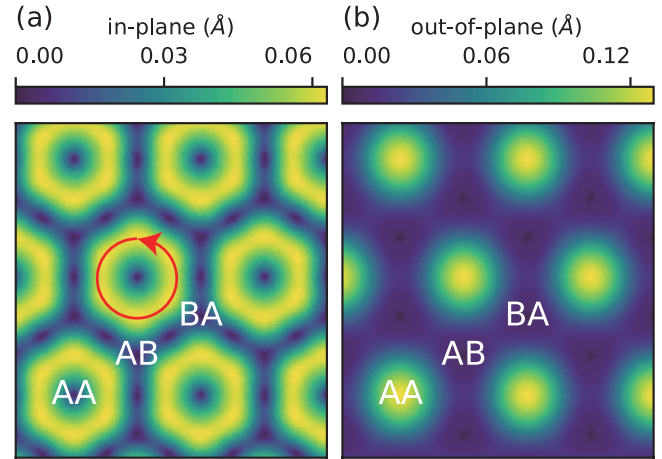


FIG. 1. Magnitude of (a) in-plane and (b) out-of-plane displacements of the upper layer after the structural relaxation in the TBG at  $\theta = 1.08^\circ$ . Red circular arrow denotes the directions of in-plane displacements. The other layer has similar displacement pattern, except that the directions are opposite. The stacking pattern of two graphene layers varies within the moiré supercell of TBG. AA-, AB-, and BA-type stacking regions are denoted by texts.

suggests that  $\lambda$  is likely to be further enhanced in low-angle twisted bilayer graphene where the flattening of Dirac cones brings large enhancements of the electron density of states. Thus, quantitative estimation of  $\lambda$  in low-angle twisted bilayer graphene can provide a valuable insight into the nature of superconductivity.

In this work, we investigate the electron-phonon interaction in MA-TBG with atomistic description of the system including more than 10,000 atoms needed for the moiré supercell. We use tight-binding approach for electrons and atomic force constants for phonons. We find that the electron-phonon coupling strength  $\lambda$  in MA-TBG is almost directly proportional to the electron den-

sity of states and becomes greater than 1 near the half-filling energies of the flat bands. It is shown that the lattice relaxations can bring electron-hole asymmetry to the electron density of states and, as a result, the hole-side flat bands have much stronger  $\lambda$  than the electron-side. We also find that the electron-phonon coupling depends very weakly on the direction and magnitude of the electronic crystal momentum. We discuss implications of our results for superconductivity in MA-TBG.

Although the electron-phonon interaction can be, in principle, obtained accurately by self-consistent density functional perturbation theory (DFPT), the large number ( $\sim 10^4$ ) of atoms in the moiré supercell is a practical barrier making DFPT calculations very difficult to achieve. In addition, considering correlation effects between electrons in atomistic description also requires challenging development due to the large number of atoms. In our present work, we employ tight-binding approach with one  $p$  orbital per carbon atom and atomic force constants for atomic vibrations without considering electron correlation effects between electrons. Our results provide fundamental understanding of electron-phonon interaction in the system obtained from atomistic description of electrons and phonons.

Moiré supercell of twisted bilayer graphene is constructed by rotating each layer of AA-stacked bilayer graphene by  $\theta/2$  and  $-\theta/2$ , respectively. The resulting atomic structure has six-fold rotation symmetry axis around  $z$ -axis, and three two-fold rotation symmetry axes that are perpendicular to  $z$ -axis, which swap two graphene layers as a result.

Preserving the crystal symmetry of nonrelaxed structure, we determine the equilibrium atomic positions by minimizing the total energy  $U$  that is the sum of in-plane strain energy and interlayer binding energy,

$$U = \frac{1}{2} \sum_{l=1}^2 \sum_{p\kappa\alpha, p'\kappa'\beta} C_{p\kappa\alpha, p'\kappa'\beta}^{\text{MLG}} \Delta\tau_{p\kappa\alpha}^l \Delta\tau_{p'\kappa'\beta}^l + \sum_{p\kappa, p'\kappa'} V_{\text{KC}}(\tau_{p\kappa}^1 - \tau_{p'\kappa'}^2). \quad (1)$$

Here  $\tau_{p\kappa\alpha}^l$  is the  $\alpha$  ( $\alpha = x, y, z$ ) component of the position of the  $\kappa$ -th atom in layer  $l$  located at the  $p$ -th moiré supercell of TBG,  $\Delta\tau_{p\kappa}^l = \tau_{p\kappa}^l - \tilde{\tau}_{p\kappa}^l$  is the deviation from the nonrelaxed position  $\tilde{\tau}_{p\kappa}^l$ , and  $C_{p\kappa\alpha, p'\kappa'\beta}^{\text{MLG}}$  are force constants between two atoms in the same layer up to fourth-nearest neighbors, taken from Ref. [57], which are obtained by fitting to the *ab initio* phonon dispersion calculations of monolayer graphene. The interlayer binding energy is calculated using Kolmogorov-Crespi (KC) potential  $V_{\text{KC}}$  that depends on interlayer atomic registry [58]. Without the interlayer binding energy, our total energy function has its minimum, by construction, at the atomic positions of the rigidly rotated two graphene layers. With the interlayer binding energy, the equilibrium

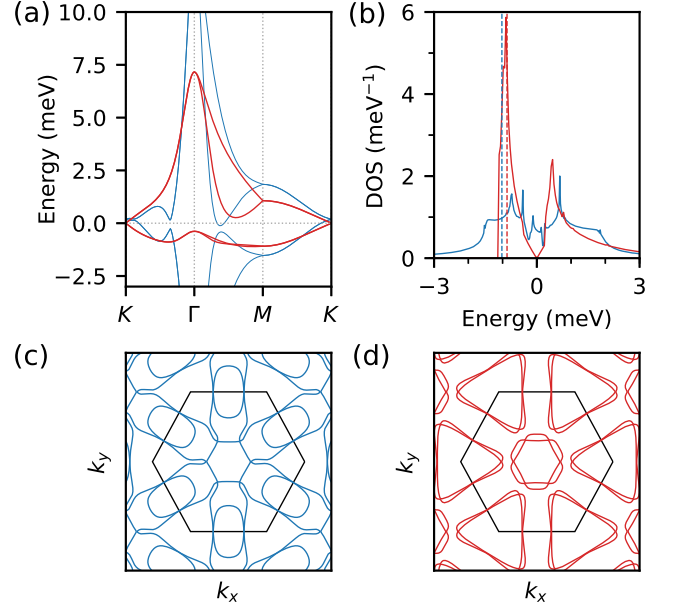


FIG. 2. Electronic structure of MA-TBG. Tight-binding (a) band structure and (b) density of states per spin for nonrelaxed (blue) and relaxed (red) structures at  $\theta = 1.08^\circ$ . Vertical dashed lines are energies that fill half of hole-side bands. (c),(d) Fermi surfaces at the energies denoted by dashed lines in (b) for nonrelaxed and relaxed structures, respectively.

atomic positions show that the area of AA-stacked regions is shrunk, while AB-stacked regions expanded, and interlayer distances in AA-stacked regions become larger than AB-stacked regions [53, 54, 59, 60].

Figure 1 shows the atomic displacements due to the relaxation at  $\theta = 1.08^\circ$ . We find that maximal out-of-plane displacements are about two times maximal in-plane displacements. Out-of-plane displacements are largest at AA-stacked region, and also noticeable at AB/BA domain boundary. The existence of locally confined strains at AB/BA domain boundaries is one of the most important consequences of the lattice relaxations in low angle TBG. Our results are consistent with the previous studies on the lattice relaxations in low angle TBG.

To investigate electronic structures of TBG in both nonrelaxed and relaxed structure, we employ single-orbital tight-binding approach where the electronic Hamiltonian is

$$\hat{H} = \sum_{p\kappa, p'\kappa'} t(\tau_{p\kappa} - \tau_{p'\kappa'}) |\phi_{p\kappa}; \mathbf{R}_p\rangle \langle \phi_{p'\kappa'}; \mathbf{R}_{p'}|, \quad (2)$$

where  $|\phi_{p\kappa}; \mathbf{R}_p\rangle$  is a carbon  $p_z$ -like orbital at  $\tau_{p\kappa}$ . Here we drop the layer index on  $\tau_{p\kappa}$ ,  $\kappa$  sweeps all the atoms in both layers, and  $\tau_{p\kappa} = \tau_{0\kappa} + \mathbf{R}_p$  for the  $p$ -th moiré supercell at  $\mathbf{R}_p$ . We use the Slater-Koster-type hopping integral,

$$t(\mathbf{d}) = V_{pp\pi}^0 e^{-(d-a_0)/\delta} \{1 - (d_z/d)^2\} + V_{pp\sigma}^0 e^{-(d-d_0)/\delta} (d_z/d)^2, \quad (3)$$

where  $\mathbf{d}$  is the displacement vector between two orbitals. The hopping energy  $V_{pp\pi}^0 = -2.7$  eV is between in-plane nearest neighbors separated by  $a_0 = a/\sqrt{3} = 1.42$  Å, and  $V_{pp\sigma}^0 = 0.48$  eV is between two vertically aligned atoms at the distance  $d_0 = 3.35$  Å. Here  $\delta = 0.184a$  is chosen to set the magnitude of the next-nearest-neighbor hopping amplitude to be  $0.1V_{pp\pi}^0$  [61, 62]. We use the cutoff distance  $d_c = 5$  Å, beyond which the hopping integral is negligible.

Figure 2(a) shows the band structures for TBLG at  $\theta = 1.08^\circ$  in the nonrelaxed and relaxed structure. One of the most noticeable effects of the lattice relaxation is the opening of the gaps at the edges of the flat bands. Furthermore, the electron-side and hole-side flat bands become significantly asymmetric due to the relaxation. The hole side gets much narrower than the electron side so that the peak height of the density of states [Fig. 2(b)] in the hole side is more than twice the electron side.

Figures 2(c) and (d) show Fermi surfaces at energies where the hole-side flat bands are half-filled for the non-relaxed and relaxed structures, respectively. At these energies, Fermi surfaces become more complicated than those near the charge-neutral energy, where only circular Fermi sheets originating from the Dirac cones are located at Brillouin zone corners. At half-filling energies, Fermi sheets at the zone corners become triangular-like, and the additional  $\Gamma$ -centered Fermi sheets appear.

Phonons in twisted bilayer graphene are calculated using atomic force constants  $C_{p\kappa\alpha,p'\kappa'\beta} = \partial^2 U / \partial \tau_{p\kappa\alpha} \partial \tau_{p'\kappa'\beta}$ , where  $U$  is given by Eq. (1). Since we treat the in-plane strain energy with the harmonic approximation, the in-plane force constants are unaltered by the lattice relaxation. The interlayer force constants, however, are evaluated at relaxed atomic positions because the KC potential [58] is not harmonic. Our approach is similar to Ref. [63], except that the Lennard-Jones interlayer potential between two graphene layers is replaced by the KC potential which can account for registry-dependent energy differences in TBG. From the force constants, we obtain the dynamical matrix  $D_{\kappa\alpha,\kappa'\beta}(\mathbf{q}) = \sum_p e^{i\mathbf{q}\cdot\mathbf{R}_p} C_{0\kappa\alpha,p\kappa'\beta} / M_C$  for phonon wavevector  $\mathbf{q}$ , where  $M_C$  is the mass of a carbon atom. Then, we solve the phonon eigenvalue problems  $\omega_{\mathbf{q}\nu}^2 e_{\mathbf{q}\nu,\kappa\alpha} = \sum_{\kappa'\beta} D_{\kappa\alpha,\kappa'\beta}(\mathbf{q}) e_{\mathbf{q}\nu,\kappa'\beta}$  at the irreducible Brillouin zone of TBG for the energy  $\omega_{\mathbf{q}\nu}$  and polarization vector  $e_{\mathbf{q}\nu,\kappa}$  of the  $\nu$ -th phonon mode. The phonons in the rest of the Brillouin zone are obtained from the symmetry relations [64].

Figure 3(a) shows phonon density of states  $F(\omega)$  for  $\theta = 1.08^\circ, 1.12^\circ$ , and  $1.16^\circ$  as well as AB-BLG. Phonon spectra are nearly insensitive to small twist angle differences. So a tiny difference is that, compared to AB-BLG, interlayer breathing modes near  $\omega \sim 11$  meV are slightly softened in TBG.

Now, we calculate the standard electron-phonon cou-

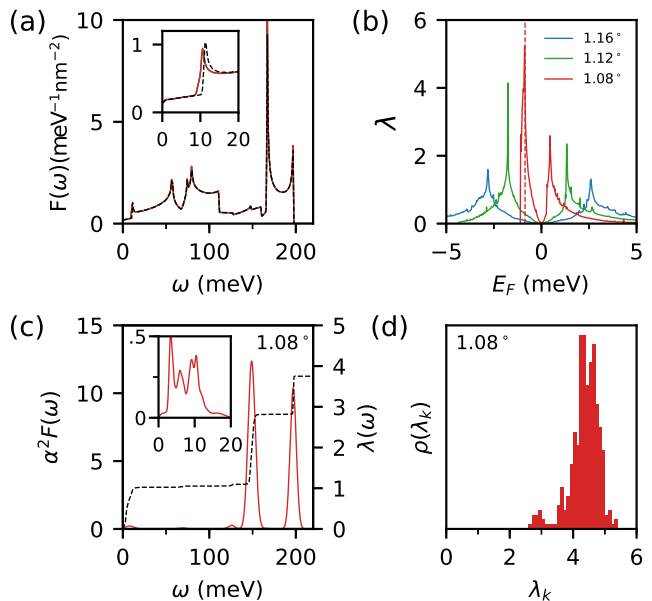


FIG. 3. (a) Phonon density of states for AB-BLG (dashed black), TBG at  $\theta = 1.08^\circ$  (solid red),  $\theta = 1.12^\circ$  (solid green), and  $\theta = 1.16^\circ$  (solid blue). Phonons are insensitive to the small twist-angle differences between those angles. The inset shows the frequency range of the interlayer shear and breathing modes, which are softened by the twist. (b) Total electron-phonon coupling strength  $\lambda$  in TBG as a function of the Fermi energy. The vertical red dashed line denotes the energy where hole-side flat bands in  $\theta = 1.08^\circ$  are half-filled. (c) Eliashberg function  $\alpha^2 F(\omega)$ , shown in red, at the half-filling energy in the hole side. The dashed black line denotes  $\lambda(\omega) = 2 \int^\omega \alpha^2 F(\omega') / \omega' d\omega'$ . The inset shows the low-frequency range of  $\alpha^2 F(\omega)$ . Phonon modes at this range contribute to about 30% of the total coupling strength. (d) Distribution of the momentum-resolved electron-phonon coupling strength  $\lambda_{\mathbf{k}}$  at the half-filling energy in the hole side.

pling strengths defined as

$$\lambda_{n\mathbf{k}} = 2N_F \sum_{m\mathbf{q}} \frac{|g_{m\nu\nu}(\mathbf{k}, \mathbf{q})|^2}{\omega_{\mathbf{q}\nu}} W_{m\mathbf{k}+\mathbf{q}}, \quad (4a)$$

$$\lambda = \sum_{n\mathbf{k}} \lambda_{n\mathbf{k}} W_{n\mathbf{k}}, \quad (4b)$$

where  $N_F$  is the electron density of states per spin at the Fermi level  $E_F$ , and  $W_{n\mathbf{k}} = \delta(E_F - \varepsilon_{n\mathbf{k}}) / N_F$  is the partial weight of the density of states. Here,  $\varepsilon_{n\mathbf{k}}$  is the electron energy of the  $n$ -th band with wavevector  $\mathbf{k}$ , and  $W_{n\mathbf{k}}$  is obtained by the linear tetrahedron method [68]. The electron-phonon matrix elements  $g_{m\nu\nu}(\mathbf{k}, \mathbf{q}) = \langle m\mathbf{k} + \mathbf{q} | \delta_{\mathbf{q}\nu} \hat{H} | n\mathbf{k} \rangle$  couples the electronic states  $|n\mathbf{k}\rangle$  and  $|m\mathbf{k} + \mathbf{q}\rangle$ , where  $\delta_{\mathbf{q}\nu} \hat{H}$  is the change in  $\hat{H}$  due to phonon mode  $(\mathbf{q}\nu)$ . The electron-phonon matrix elements in localized orbital basis can be expressed in terms of the changes in the hopping matrix elements due to the atomic

displacements of phonon modes [65–67],

$$g_{mn\nu}(\mathbf{k}, \mathbf{q}) = l_{q\nu} \sum_{\kappa\alpha} e_{q\nu,\kappa\alpha} \sum_{pp',ij} e^{-i(\mathbf{k}+\mathbf{q})\cdot\mathbf{R}_{p'}} e^{i\mathbf{k}\cdot\mathbf{R}_p} \\ \times c_{m\mathbf{k}+\mathbf{q},j}^* c_{n\mathbf{k},i} \langle \phi_j; \mathbf{R}_{p'} | \frac{\partial \hat{H}}{\partial \tau_{0\kappa\alpha}} | \phi_i; \mathbf{R}_p \rangle, \quad (5)$$

where  $l_{q\nu} = \sqrt{\hbar/(2M_C\omega_{q\nu})}$  is the length scale of phonon mode ( $q\nu$ ), and  $c_{n\mathbf{k},i}$  is coefficient of the electron wavefunctions in local orbital basis, i.e.,  $c_{n\mathbf{k},i} e^{i\mathbf{k}\cdot\mathbf{R}_p} = \sqrt{N} \langle \phi_i; \mathbf{R}_p | n\mathbf{k} \rangle$ . Here,  $N$  is the total number of unit cells over which the electronic states are normalized. Thus, in our tight-binding approach, we obtain the electron-phonon matrix elements

$$g_{mn\nu}(\mathbf{k}, \mathbf{q}) = l_{q\nu} \sum_{\kappa\alpha} e_{q\nu,\kappa\alpha} \sum_{p,i} \frac{\partial}{\partial x_\alpha} t(\tau_{0\kappa} - \tau_{pi}) \\ \times \{ e^{i\mathbf{k}\cdot\mathbf{R}_p} c_{m\mathbf{k}+\mathbf{q},\kappa}^* c_{n\mathbf{k},i} + e^{-i(\mathbf{k}+\mathbf{q})\cdot\mathbf{R}_p} c_{m\mathbf{k}+\mathbf{q},i}^* c_{n\mathbf{k},\kappa} \}. \quad (6)$$

When we apply our method to calculate  $\lambda$  for simple monolayer graphene and AB-BLG,  $\lambda$  is less than 0.1 near the charge-neutral energy but it increases up to  $0.2 \sim 0.3$  in proportion to the density of states when the chemical potential is varied. This is consistent with the previous studies for monolayer and bilayer graphene [56, 69, 70]

Figure 3(b) shows calculated electron-phonon coupling strength as a function of the Fermi energy for the three twist angles.  $\mathbf{k}$ - and  $\mathbf{q}$ -grids of  $30 \times 30$  in the moiré Brillouin zone are used for electrons and phonons. Due to the large density of states of the flat bands,  $\lambda$  becomes extremely large as  $\theta$  approaches  $1.08^\circ$ , where the Dirac cones are nearly flat. Furthermore, as the lattice relaxation brings electron-hole asymmetry in the density of states, the maximum value of  $\lambda$  is almost two times larger in the hole-side flat bands. Figure 3(c) shows the isotropic Eliashberg functions  $\alpha^2 F(\omega) = \frac{1}{N_F} \sum_{nm\nu\mathbf{k}\mathbf{q}} |g_{mn\nu}(\mathbf{k}, \mathbf{q})|^2 \delta(E_F - \varepsilon_{n\mathbf{k}}) \delta(E_F - \varepsilon_{m\mathbf{k}+\mathbf{q}}) \delta(\omega - \omega_{q\nu})$  at the half-filling energies of the hole-side flat bands in  $\theta = 1.08^\circ$ . High-energy optical modes generate strong peaks at 150 meV and 200 meV in  $\alpha^2 F(\omega)$ . Although the interlayer shear ( $\sim 2$  meV) and breathing modes ( $\sim 11$  meV) have order of magnitude smaller values of  $\alpha^2 F(\omega)$  than the in-plane optical modes, they have significant contributions to the total electron-phonon coupling strength due to their low-phonon energies. We also find that the electron-phonon coupling constant  $\lambda_{\mathbf{k}}$  is nearly isotropic and very weakly dependent on the electronic crystal momentum [Fig. 3(d)], which suggests single-gap  $s$ -wave superconductivity.

In conventional phonon-mediated superconductors, transition temperature can be reliably calculated from the Migdal-Eliashberg equations [71, 72]. But the validity of the Migdal-Eliashberg theory depends on the existence of small parameter  $\omega_{ph}/E_F \ll 1$  where  $\omega_{ph}$  is relevant phonon energy scale. This condition is obviously violated in magic-angle twisted bilayer graphene. For instance, while  $E_F \approx 1$  meV near the half-fillings of the

flat bands,  $\omega_{ph} \approx 2 \sim 11$  meV for the interlayer shear and breathing modes, and  $\omega_{ph} \approx 150 \sim 170$  meV for the in-plane optical modes. In this sense, MA-TBG systems is close to the adiabatic limit  $\omega_{ph}/E_F \gg 1$ .

Superconducting transition temperature in the antiadiabatic limit has been studied in several literatures [74–78], where the prefactor of the superconducting transition temperature is determined by the electron Fermi energy instead of the phonon energy [76, 78], that is,

$$T_c \sim E_F \exp(-1/\lambda). \quad (7)$$

In our calculations for  $\theta = 1.08^\circ$ ,  $\lambda = 3.6$  (0.56) at  $E_F = 0.86$  (1.02) meV where the hole-side (electron-side) flat bands are half-filled. These values give  $T_c \sim 7.5$  K for the hole side and  $T_c \sim 1.9$  K for the electron side. Although our estimation is crude for direct comparison with experiments, the order of magnitude is close to the experimentally observed  $T_c \sim 1.7$  K in the hole side. Since our estimation does not take into account the effect of Coulomb interaction, which can reduce  $T_c$ , we expect that calculating  $T_c$  including the Coulomb effect can give more consistent results to the experimental situations. Also, the rapid energy dependence of the electronic density of states can play an important role in determining the transition temperature [79].

In conclusion, we have calculated the electron-phonon coupling strength in the magic-angle twisted bilayer graphene using atomistic description of electrons and phonons. Obtained  $\lambda$  in MA-TBG becomes almost an order of magnitude larger than that in simple monolayer or unrotated bilayer graphene. For  $\theta = 1.08^\circ$ , the electron-hole asymmetry arises from atomic-structure relaxation due to interlayer interaction so that the electron-phonon coupling is stronger in the hole-side flat bands. The electron-phonon interaction is almost isotropic and has very weak dependence on the electron momentum, suggesting single-gap  $s$ -wave superconductivity. We also found that MA-TBG is in the antiadiabatic limit where the electron energy scale is much smaller than the phonon energy scale. Although  $T_c$  formula in the antiadiabatic limit was tried to produce values of  $T_c$  comparable to the experiments, theory of  $T_c$  of the system may require including Coulomb interaction and rapid energy dependence of the electronic density of states as well as electron correlation and any possible presence of magnetic fluctuations. Our results provide fundamental understanding of electron-phonon interaction in MA-TBG obtained from atomistic description of electrons and phonons, highlighting that it can contribute to rich physics of the system.

This work was supported by NRF of Korea (Grant No. 2011-0018306). Y.W.C. acknowledges support from NRF of Korea (Global Ph.D. Fellowship Program NRF-2017H1A2A1042152). Computational resources have been provided by KISTI Supercomputing Center (Projects No. KSC-2017-C3-0079).

- 
- \* h.j.choi@yonsei.ac.kr
- [1] T. de Laissardière, Mayou, and Magaud, Localization of Dirac Electrons in Rotated Graphene Bilayers, *Nano Lett.* **10**, 804 (2010).
  - [2] E. S. Morell, J. D. Correa, P. Vargas, M. Pacheco, and Z. Barticevic, Flat bands in slightly twisted bilayer graphene: Tight-binding calculations, *Phys. Rev. B* **82**, 121407 (2010).
  - [3] R. Bistritzer and A. MacDonald, Moiré bands in twisted double-layer graphene, *Proc. Natl. Acad. Sci. U.S.A.* **108**, 12233 (2011).
  - [4] Y. Cao, V. Fatemi, A. Demir, S. Fang, S. L. Tomarken, J. Y. Luo, J. D. Sanchez-Yamagishi, K. Watanabe, T. Taniguchi, E. Kaxiras, R. C. Ashoori, and P. Jarillo-Herrero, Correlated insulator behaviour at half-filling in magic-angle graphene superlattices, *Nature* **556**, 80 (2018).
  - [5] Y. Cao, V. Fatemi, S. Fang, K. Watanabe, T. Taniguchi, E. Kaxiras, and P. Jarillo-Herrero, Unconventional superconductivity in magic-angle graphene superlattices, *Nature* **556**, 43 (2018).
  - [6] H. Guo, X. Zhu, S. Feng, and R. T. Scalettar, Pairing symmetry of interacting fermions on a twisted bilayer graphene superlattice, *Phys. Rev. B* **97**, 235453 (2018).
  - [7] J. F. Dodaro, S. A. Kivelson, Y. Schattner, X. Q. Sun, and C. Wang, Phases of a phenomenological model of twisted bilayer graphene, *Phys. Rev. B* **98**, 075154 (2018).
  - [8] M. Fidrysiak, M. Zegrodnik, and J. Spałek, Unconventional topological superconductivity and phase diagram for an effective two-orbital model as applied to twisted bilayer graphene, *Phys. Rev. B* **98**, 085436 (2018).
  - [9] T.-F. Chung, Y. Xu, and Y. P. Chen, Transport measurements in twisted bilayer graphene: Electron-phonon coupling and Landau level crossing, *Phys. Rev. B* **98**, 035425 (2018).
  - [10] M. Ochi, M. Koshino, and K. Kuroki, Possible correlated insulating states in magic-angle twisted bilayer graphene under strongly competing interactions, *Phys. Rev. B* **98**, 081102 (2018).
  - [11] A. Thomson, S. Chatterjee, S. Sachdev, and M. S. Scheurer, Triangular antiferromagnetism on the honeycomb lattice of twisted bilayer graphene, *Phys. Rev. B* **98**, 075109 (2018).
  - [12] L. Zou, H. C. Po, A. Vishwanath, and T. Senthil, Band structure of twisted bilayer graphene: Emergent symmetries, commensurate approximants, and Wannier obstructions, *Phys. Rev. B* **98**, 085435 (2018).
  - [13] X. Lin and D. Tománe, Minimum model for the electronic structure of twisted bilayer graphene and related structures, *Phys. Rev. B* **98**, 081410 (2018).
  - [14] S. Carr, S. Fang, P. Jarillo-Herrero, and E. Kaxiras Pressure dependence of the magic twist angle in graphene superlattices, *Phys. Rev. B* **98**, 085144 (2018).
  - [15] M. Anđelković, L. Covaci, and F. M. Peeters, DC conductivity of twisted bilayer graphene: Angle-dependent transport properties and effects of disorder, *Phys. Rev. Materials* **2**, 034004 (2018).
  - [16] H. Chun Po, L. Zou, A. Vishwanath, and T. Senthil, Origin of Mott insulating behavior and superconductivity in twisted bilayer graphene, arXiv:1803.09742.
  - [17] B. Roy and V. Juricic, Unconventional superconductivity in nearly flat bands in twisted bilayer graphene, arXiv:1803.11190.
  - [18] G. Baskara, Theory of emergent Josephson lattice in neutral twisted bilayer graphene (Moiré is different), arXiv:1804.00627.
  - [19] B. Padhi, C. Setty, and P. W. Phillips, Doped twisted bilayer graphene near magic angles: proximity to Wigner crystallization not Mott insulation, arXiv:1804.01101.
  - [20] T. Huang, L. Zhang, and T. Ma, Antiferromagnetically ordered Mott insulator and d+id superconductivity in twisted bilayer graphene: A quantum Monte carlo study, arXiv:1804.06096.
  - [21] L. Zhang, Low-energy moire band formed by Dirac zero modes in twisted bilayer graphene, arXiv:1804.09047.
  - [22] S. Ray and T. Das, Wannier pairs in the superconducting twisted bilayer graphene and related systems, arXiv:1804.09674.
  - [23] C.-C. Liu, L.-D. Zhang, W.-Q. Chen, and F. Yang, Chiral SDW and d + id superconductivity in the magic-angle twisted bilayer-graphene, arXiv:1804.10009.
  - [24] X. Y. Xu, K. T. Law, and P. A. Lee, Kekulé valence order in an extended Hubbard model on the honeycomb lattice with possible applications to twisted bilayer graphene, *Phys. Rev. B* **98**, 121406 (2018).
  - [25] T. J. Peltonen, R. Ojajarvi, and T. T. Heikkila, Mean-field theory for superconductivity in twisted bilayer graphene, arXiv:1805.01039.
  - [26] J.-B. Qiao and L. He, Heterostrain engineering on twisted graphene bilayer around the first magic angle, arXiv:1805.03790.
  - [27] J. Kang and O. Vafek, Symmetry, maximally localized Wannier states, and low energy model for the twisted bilayer graphene narrow bands, arXiv:1805.04918.
  - [28] L. Rademaker and P. Mellado, Charge-transfer insulation in twisted bilayer graphene, arXiv:1805.05294.
  - [29] D. M. Kennes, J. Lischner, and C. Karrasch, Strong correlations and d+id superconductivity in twisted bilayer graphene, arXiv:1805.06310.
  - [30] H. Isobe, N. F. Q. Yuan, and L. Fu, Unconventional superconductivity and density waves in twisted bilayer graphene, arXiv:1805.06449.
  - [31] M. Koshino, N. F. Q. Yuan, T. Koretsune, M. Ochi, K. Kuroki, and L. Fu, Maximally-localized Wannier orbitals and the extended Hubbard model for the twisted bilayer graphene, arXiv:1805.06819.
  - [32] Y.-Z. You and A. Vishwanath, Superconductivity from valley fluctuations and approximate SO(4) symmetry in a weak coupling theory of twisted bilayer graphene, arXiv:1805.06867.
  - [33] J. M. Pizarro, M. J. Calderon, and E. Bascones, The nature of correlations in the insulating states of twisted bilayer graphene, arXiv:1805.07303.
  - [34] F. Wu, A. H. MacDonald, and I. Martin, Theory of phonon-mediated superconductivity in twisted bilayer graphene, arXiv:1805.08735.
  - [35] H. K. Pal, On magic angles and band flattening in twisted bilayer graphene, arXiv:1805.08803.
  - [36] F. Guinea and N. R. Walet, Electrostatic effects and band distortions in twisted graphene bilayers, arXiv:1806.05990.
  - [37] J. Gonzalez and T. Staube, Kohn-Luttinger superconductivity in twisted bilayer graphene, arXiv:1807.01275.
  - [38] Ying Su and Shi-Zeng Li, Spontaneous vortex-antivortex

- lattice in superconducting twisted bilayer graphene, arXiv:1807.02196.
- [39] B. Lian, Z. Wang, and B. A. Bernevig, Twisted bilayer graphene: a phonon driven superconductor, arXiv:1807.04382.
- [40] Y. Sherkunov and J. J. Betouras, Novel phases in twisted bilayer graphene at magic angles as a result of van Hove singularities and interactions, arXiv:1807.05524.
- [41] A. O. Sboychakov, A. V. Rozhkov, A. L. Rakhmanov, and F. Nori, Many-body effects in twisted bilayer graphene at low twist angles, arXiv:1807.08190.
- [42] B. L. Chittari, N. Leconte, S. Javvaji, and J. Jung, Pressure induced compression of flatbands in twisted bilayer graphene, arXiv:1808.00104.
- [43] K. Hejazi, C. Liu, H. Shapourian, X. Chen, and L. Balents, Multiple topological transitions in twisted bilayer graphene near the first magic angle, arXiv:1808.01568.
- [44] X. Lin and D. Tománek, Minimum model for the electronic structure of twisted bilayer graphene and related structures, Phys. Rev. B **98**, 081410 (2018).
- [45] E. Laksono, J. N. Leaw, A. Reaves, M. Singh, X. Wang, S. Adam, and X. Gu, Singlet superconductivity enhanced by charge order in nested twisted bilayer graphene Fermi surfaces, Solid State Commun. **282**, 38 (2018).
- [46] G. Tarnopolsky, A. J. Kruchkov, and A. Vishwanath, Origin of magic angles in twisted bilayer graphene, arXiv:1808.05250.
- [47] J. Ahn, S. Park, and B.-J. Yang, Failure of Nielsen-Ninomiya theorem and fragile topology in two-dimensional systems with space-time inversion symmetry: application to twisted bilayer graphene at magic angle, arXiv:1808.05375.
- [48] M. Yankowitz, S. Chen, H. Polshyn, K. Watanabe, T. Taniguchi, D. Graf, A. F. Young, and C. R. Dean, Tuning superconductivity in twisted bilayer graphene, arXiv:1808.07865.
- [49] J. W. F. Venderbos and R. M. Fernandes, Correlations and electronic order in a two-orbital honeycomb lattice model for twisted bilayer graphene, arXiv:1808.10416.
- [50] L. Chen, H.-Z. Li, and R.-S. Han, Magnetic-impurity resonance states for different pairing symmetries in twisted bilayer graphene, arXiv:1809.00436.
- [51] T. Stauber, T. Low, and G. Gómez-Santo, Linear response of twisted bilayer graphene: continuum vs. tight-binding models, arXiv:1809.03465.
- [52] Q. K. Tang, L. Yang, D. Wang, F. C. Zhang, and Q. H. Wang, Spin-triplet f-wave pairing in twisted bilayer graphene near 1/4 filling, arXiv:1809.06772.
- [53] H. Yoo, K. Zhang, R. Engelke, P. Cazeaux, S. H. Sung, R. Hovden, A. W. Tsen, T. Taniguchi, K. Watanabe, G.-C. Yi, M. Kim, M. Luskin, E. B. Tadmor, and P. Kim, Atomic reconstruction at van der Waals interface in twisted bilayer graphene, arXiv:1804.03806.
- [54] N. N. T. Nam and M. Koshino, Lattice relaxation and energy band modulation in twisted bilayer graphene, Phys. Rev. B **96**, 075311 (2017).
- [55] Y. Cao, J. Y. Luo, V. Fatemi, S. fang, J. D. Sanchez-Yamagishi, K. Watanabe, T. Taniguchi, E. Kaxiras, and P. Jarillo-Herrero, Superlattice-induced insulating states and valley-protected orbits in twisted bilayer graphene, Phys. Rev. Lett. **117**, 116804 (2016).
- [56] C.-H. Park, F. Giustino, M. L. Cohen, and S. G. Louie, Electron-Phonon Interactions in Graphene, Bilayer Graphene, and Graphite, Nano Lett. **8**, 4229 (2008).
- [57] L. Wirtz and A. Rubio, The phonon dispersion of graphite revisited, Solid State Commun. **131**, 141 (2004).
- [58] A. N. Kolmogorov and V. H. Crespi, Registry-dependent interlayer potential for graphitic systems, Phys. Rev. B **71**, 235415 (2005).
- [59] K. Zhang and E. B. Tadmor, Energy and moiré patterns in 2D bilayers in translation and rotation: A study using an efficient discrete-continuum interlayer potential, Extreme Mechanics Letters **14**, 16 (2017).
- [60] K. Zhang and E. B. Tadmor, Structural and electron diffraction scaling of twisted graphene bilayers, J. Mech. Phys. Solids **112**, 225 (2018).
- [61] P. Moon and M. Koshino, Energy spectrum and quantum Hall effect in twisted bilayer graphene, Phys. Rev. B **85**, 195458 (2012).
- [62] T. Nakanishi and T. Ando, Conductance of crossed carbon nanotubes, J. Phys. Soc. Jpn. **70**, 1647 (2001).
- [63] A. Cocemasov, D. Nika, and A. Balandin, Phonons in twisted bilayer graphene, Phys. Rev. B **88**, 035428 (2013).
- [64] A. A. Maradudin and S. H. Vosko, Symmetry properties of the normal vibrations of a crystal, Rev. Mod. Phys. **40**, 1 (1968).
- [65] F. Giustino, M. L. Cohen, and S. G. Louie, Electron-phonon interaction using Wannier functions, Phys. Rev. B **76**, 165108 (2007).
- [66] T. Gunst, T. Markussen, K. Stokbro, and M. Brandbyge, First-principles method for electron-phonon coupling and electron mobility: Applications to two-dimensional materials, Phys. Rev. B **93**, 035414 (2016).
- [67] L. A. Agapito and M. Bernadi, *Ab initio* electron-phonon interactions using atomic orbital wave functions, Phys. Rev. B **97**, 235146 (2018).
- [68] P. E. Blöchl, O. Jepsen, and O. K. Andersen, Improved tetrahedron method for Brillouin-zone integrations, Phys. Rev. B **49**, 16223 (1994).
- [69] M. Bianchi, E. D. L. Rienks, S. Lizzit, A. Baraldi, R. Balog, L. Hornekær, and P. Hofmann, Electron-phonon coupling in potassium-doped graphene: Angle-resolved photoemission spectroscopy, Phys. Rev. B **81**, 041403 (2010).
- [70] J. C. Johannsen, S. Ulstrup, M. Bianchi, R. Hatch, D. Guan, F. Mazzola, L. Hornekær, F. Fromm, C. Raidel, T. Seyller, and P. Hofmann, Electron-phonon coupling in quasi-free-standing graphene, J. Phys.: Condens. Matter **25**, 094001 (2013).
- [71] A. B. Migdal, Interaction between electrons and lattice vibrations in a normal metal, Sov. Phys. JETP **7**, 996 (1958).
- [72] G. M. Eliashberg, Interactions between electrons and lattice vibrations in a superconductor, Sov. Phys. JETP **11**, 696 (1960).
- [73] P. B. Allen and R. C. Dynes, Transition temperature of strong-coupled superconductors reanalyzed, Phys. Rev. B **12**, 905 (1975).
- [74] D. M. Eagles, Predicted Transition Temperatures of Very Thin Films and Whiskers of Superconducting Semiconductors - Application to SrTiO<sub>3</sub>, Phys. Rev. **164**, 489 (1967).
- [75] M. A. Ikeda, A. Ogasawara, and M. Sugihara, On Migdal's theorem, Phys. Lett. A **170**, 319 (1992).
- [76] L. P. Gor'kov, Superconducting transition temperature: Interacting Fermi gas and phonon mechanisms in the nonadiabatic regime, Phys. Rev. B **93**, 054517 (2016).

- [77] L. P. Gor'kov, Phonon mechanism in the most dilute superconductor n-type SrTiO<sub>3</sub>, Proc. Natl. Acad. Sci. U.S.A. **113**, 4646 (2016).
- [78] M. V. Sadoskii, Electron-phonon coupling in Eliashberg-McMillan theory beyond adiabatic approximation, arXiv:1809.02531.
- [79] P. B. Allen and B. Mitrović, in Solid State Physics, edited by H. Ehrenreich, F. Seitz, and D. Turnbull (Academic, New York, 1982), Vol. 37, p. 1.